Liu *et al.*
Chinese Journal of Mechanical Engineering (2022) 35:130
https://doi.org/10.1186/s10033-022-00801-5

Chinese Journal of Mechanical Engineering

ORIGINAL ARTICLE

Open Access

Optimal Design and Experimental Verification of Low Radiation Noise of Gearbox

Lan Liu[1*], Kun Kang[1], Yingjie Xi[1], Zhengxi Hu[1,2], Jingyi Gong[1] and Geng Liu[1]

Abstract

Reducing the radiated noise of a gearbox is a difficult problem in aviation, navigation, machinery, and other fields. Structural improvement is the main means of noise reduction for a gearbox, and it is realized primarily through contribution analysis and structure optimization. However, these approaches have certain limitations. In this study, a low-noise design method for a gearbox that combines the two approaches is proposed, and experimental verification is performed. First, a finite element/boundary element model is established using a single-stage herringbone gearbox. Considering the vibration excitation of the gear system, the radiation noise of a single-stage gearbox is predicted based on the modal acoustic transfer vector (MATV) method. Subsequently, the maximum field point of the radiated noise is determined, and the acoustic transfer vector (ATV) analysis and modal acoustic contribution (MAC) analysis are conducted to determine the region that contributes significantly to the radiated noise of the field point. The optimization region is selected through the panel acoustic contribution (PAC) analysis. Next, to reduce the normal speed in the optimization region, topology optimization is performed. According to the topology optimization results, four different noise reduction structures are added to the gearbox, and the low-noise optimization models are established respectively. Finally, by measuring the radiated noise of the gearbox before and after optimization under a given working condition, the validity of the radiated noise prediction method and the low-noise optimization design method are verified by comparing the simulation and experimental data. A comparison of the four optimization models proves that the noise reduction effect can be achieved only by adding a noise reduction structure to the center of the density nephogram.

Keywords: Radiated noise prediction, Acoustic contribution analysis, Topology optimization, Noise reduction structures, Experimental verification

1 Introduction

The vibration of the gear system in a gearbox transmits the excitation to the box body through the bearing seat, which not only causes the gearbox to generate radiation noise to the outside and affect the cabin comfort, but also further transmits the vibration to the hull through the bolt of the box foot, thus posing a threat to the safety of the ship. Therefore, it is crucial to reduce the noise pollution of the gearbox by choosing appropriate noise-reduction methods based on the accurate prediction of radiated noise. At present, the noise reduction measures adopted by ships at home and abroad for gearboxes primarily include [1] structural improvement design of gearboxes, laying of damping materials, and noise active control. Currently, there are two methods for improving the gearbox structure to reduce vibration and noise: acoustic contribution analysis and structural optimization.

The main idea of acoustic contribution analysis is to determine the position that contributes significantly to the radiated noise of the field point, which is the main region for structural improvement, and to complete the

*Correspondence: liulan@nwpu.edu.cn

[1] Shaanxi Engineering Laboratory for Transmissions and Controls, School of Mechanical Engineering, Northwestern Polytechnical University, Xi'an 710072, China
Full list of author information is available at the end of the article

structural improvement to reduce the sound pressure value of this field point. Panel contribution analysis was first applied to noise reduction in vehicles [2] and has been applied to vibration and noise reduction of gearboxes in recent years [3, 4]. Liu [5] used real car data acquisition, comprehensive simulation calculation and the establishment of a sound quality prediction model to obtain the acoustic mode of an indoor acoustic cavity. Furthermore, the data was used to analyze and compare the contribution of the body panel based on the sound pressure level and sound quality. Through modal acoustic contribution (MAC) analysis, the mode that contributes significantly to the radiation noise of a certain field point can be determined and the structure of the region where the bending mode appears can be improved, which can reduce the radiation noise of this field point [6]. Wang et al. [7] combined PAC and MAC analyses and proposed a method that can quickly and accurately determine the effective improvement region, and the structural improvement of this region can significantly reduce the radiated noise of the gearbox. Aiming at the problem of radiated noise in automobile transmission housing, Zong et al. [8] proposed a method to determine the specific location of the shell that needs to be improved intuitively and accurately using MAC and PAC analyses. Additionally, the improved shell structure can effectively improve the noise characteristics of the shell.

Structural optimization primarily includes size, morphology and topology optimization. Topology optimization offers more design freedom to designers, thereby allowing them to obtain better results than other optimization methods [9]; therefore, this method is widely used in aviation [10, 11], aerospace [12], machinery [13], vehicles [14, 15], mechanism design [16, 17], structural design [18, 19] and other fields. The homogenization [20, 21], variable density [22], and level set methods [23, 24] are the main methods used to solve topology optimization. Of these, the variable-density method is commonly used. Park et al. [25] used an air compressor as an example to determine the modal order that has the greatest influence on the noise peak value through experiments; subsequently, they optimized the topology with the maximum natural frequency corresponding to this modal as the goal. After the optimization, the radiated noise was reduced.

In the above two methods of acoustic contribution analysis and topology optimization, the goal of topology optimization is clear and the constraints are accurate, but it is difficult to select the design domain. Therefore, it obtains good optimization results while bringing a large amount of calculation. The acoustic contribution analysis can determine a certain region that contributes significantly to radiation noise. Although its calculation scale is small, it cannot obtain an accurate improvement method. In summary, if the design domain can be selected through contribution analysis, and accurate optimization results can be obtained through topology optimization, then the advantages of both can be applied. Some studies have been conducted in this field. Shu et al. [26] determined the regions with large contributions through PAC analysis and maximized the first-order natural frequency through topology and morphology optimization, which significantly reduced the radiated noise after optimization. Li et al. [27] aimed to improve the third-order natural frequency and reduce the noise emissivity in this region and obtained an optimal wall thickness scheme to significantly reduce the noise in the optimized region. Zhang et al. [28] used the body wall panel noise and modal contributions as a comprehensive evaluation index to establish a multi-objective optimization function of the dynamic mechanical properties of the body panel, and a topology optimization technique was used to obtain the optimal layout of the damping material.

In this study, the radiation noise prediction, low-noise optimization design, and gearbox experiment were studied. In Section 2, the definitions of ATV (acoustic transfer vector), MATV (modal acoustic transfer vector), MAC, PAC, and topology optimization are introduced. In Section 3, using a single-stage herringbone gearbox as the research object, a finite element/boundary element model of the gearbox is established and its radiated noise is predicted under the excitation of a certain working condition. In Section 4, ATV, MAC and PAC analyses are performed to screen out the panel region, which contributes significantly to the radiated noise of the target field. Subsequently, according to the topology optimization results, by adding noise reduction structures, a low-noise optimization model of the gearbox is established. In Section 5, the radiated noise of the gearbox before and after optimization is measured in a semi-anechoic chamber. The results show that the low-noise optimization design method can effectively reduce the radiated noise of the target optimization field points.

2 Theoretical Basis

2.1 ATV and MATV

The acoustic equation can be regarded as linear under the condition of a small pressure disturbance, and a linear relationship can be established between the sound pressure at a certain field point in the sound field and the vibration at the structural surface; thus, the sound pressure at any position $\boldsymbol{r}$ in the sound field at frequency ω is as shown in Eq. (1) [29].

$$\boldsymbol{p}(\boldsymbol{r},\omega) = \{\boldsymbol{ATV}(\boldsymbol{r},\omega)\}^{\mathrm{T}}\{\boldsymbol{v_n}(\omega)\}, \tag{1}$$

where $\{\boldsymbol{ATV}(\boldsymbol{r},\omega)\}$ denotes the acoustic transfer vector; $\boldsymbol{v}_n$ denotes the vibration velocity in the normal direction of the structural surface; ω denotes the angular frequency.

Therefore, the physical meaning of the $\boldsymbol{ATV}$ can be understood as the sound pressure value caused by the unit speed of an element or node at a certain field point at a specific frequency.

The main factors affecting ATV include [29]: (a) the shape of the closed boundary, which is the surface shape of the structure; (b) the value of Green's function; hence, the position of the field point is one of the main factors affecting the ATV; (c) physical parameters of the acoustic medium (including density, wave velocity, etc.); and (d) calculation and analysis frequency of radiated noise.

In addition, through the linear superposition of the mode shape, the displacement response of the structural vibration can be expressed as

$$\{\boldsymbol{u}(\omega)\} = \boldsymbol{\Omega}\{\boldsymbol{MRSP}(\omega)\}, \tag{2}$$

where $\{\boldsymbol{u}\}$ is the displacement of the structure; $\boldsymbol{\Omega}$ is a matrix formed by the structural modal vector; $\{\boldsymbol{MRSP}(\omega)\}$ is a vector formed by the modal participation factor.

The displacement vector of the structure $\{\boldsymbol{u}\}$ is projected in the normal direction of the structure surface, and the vibration velocity in the normal direction can be expressed as

$$\{\boldsymbol{v_n}(\omega)\} = j\omega\, \boldsymbol{\Omega_n}\{\boldsymbol{MRSP}(\omega)\}, \tag{3}$$

where $\boldsymbol{\Omega_n}$ is a matrix composed of component vectors of the vibration modes in the normal direction of the structural surface.

Eq. (3) is substituted into Eq. (1) to obtain the sound pressure at any point in the sound field, as Eq. (4).

$$\begin{aligned}\boldsymbol{p}(\boldsymbol{r},\omega) &= \{\boldsymbol{ATV}(\boldsymbol{r},\omega)\}^{\mathrm{T}} \cdot i\omega \cdot \boldsymbol{\Omega_n} \cdot \{\boldsymbol{MRSP}(\omega)\} \\ &= \{\boldsymbol{MATV}(\boldsymbol{r},\omega)\}^{\mathrm{T}}\{\boldsymbol{MRSP}(\omega)\},\end{aligned} \tag{4}$$

where $\{\boldsymbol{MATV}(\boldsymbol{r},\omega)\}^{\mathrm{T}}$ is the modal acoustic transfer vector, and its expression is:

$$\{\boldsymbol{MATV}(\boldsymbol{r},\omega)\}^{\mathrm{T}} = \{\boldsymbol{ATV}(\boldsymbol{r},\omega)\}^{\mathrm{T}} \cdot i\omega \cdot \boldsymbol{\Omega_n}. \tag{5}$$

The physical meaning of $\{\boldsymbol{MATV}(\boldsymbol{r},\omega)\}$ can be understood as the sound pressure value at a certain point in the sound field based on a single modal response at a specific frequency.

2.2 MAC

Eq. (3) can be expanded to obtain the normal vibration velocity of a structure [30].

$$\boldsymbol{v_n}(\omega) = i\omega \sum_{j=1}^{N} \boldsymbol{Q_j}(\omega)\varphi_{\boldsymbol{nj}}, \tag{6}$$

where $\varphi_{\mathbf{nj}}$ is the normal component of the jth structural modal shape on the surface; and N is the total order of the structural mode of participation calculation.

Substituting Eq. (6) in Eq. (1), the sound pressure at any point in the sound field in the frequency domain can be obtained, as shown in Eq. (7).

$$\begin{aligned}\boldsymbol{p}(\boldsymbol{r},\omega) &= \boldsymbol{ATV}(\boldsymbol{r},\omega)^{\mathrm{T}} i\omega \sum_{j=1}^{N} \boldsymbol{Q_j}(\omega)\boldsymbol{\varphi_{nj}} \\ &= \sum_{j=1}^{N} i\omega \boldsymbol{Q_j}(\omega)\boldsymbol{ATV}(\boldsymbol{r},\omega)^{\mathrm{T}}\varphi_{\boldsymbol{nj}} \\ &= \sum_{j=1}^{N} \boldsymbol{p_{sj}}(\boldsymbol{r},\omega),\end{aligned} \tag{7}$$

where $\boldsymbol{p_{sj}(r,\omega)}$ is the sound pressure produced by the jth structure mode.

The total sound pressure at any field point in the sound field can be obtained by superimposing the sound pressures caused by various modes of the structure. $D_{sj}(\boldsymbol{r},\omega)$ as shown in Eq. (8) is the acoustic contribution of the jth structural mode.

$$D_{sj}(\boldsymbol{r},\omega) = \frac{\left|\boldsymbol{p_{sj}}(\boldsymbol{r},\omega)\right| \cos(\theta_p - \theta_{pj})}{|\boldsymbol{p}(\boldsymbol{r},\omega)|}, \tag{8}$$

where θ_p and θ_{pj} are the phases of $\boldsymbol{p}(\boldsymbol{r},\omega)$ and $\boldsymbol{p_{sj}}(\boldsymbol{r},\omega)$, respectively.

The physical meaning of MAC is the proportion of sound pressure produced by the jth structure mode to the total sound pressure. If the acoustic contribution of a certain structure mode is greater, the influence of this mode on the total sound pressure is greater. When the acoustic contribution $D_{sj}(\boldsymbol{r},\omega)$ of a certain structural mode is larger, it shows that a certain structure has a larger mode participation factor $\boldsymbol{Q_j}(\omega)$. According to Eq. (6), the structure exhibits a larger normal vibration velocity in this mode.

2.3 PAC

By expanding $\boldsymbol{ATV}(\boldsymbol{r},\omega)$ and $\varphi_{\boldsymbol{nj}}$, Eq. (7) can be converted into the form shown by Eq. (9).

$$\begin{aligned}\boldsymbol{p}(\boldsymbol{r},\omega) &= \sum_{j=1}^{N} i\omega \boldsymbol{Q_j}(\omega) \sum_{k=1}^{m} \boldsymbol{ATV_k}(\boldsymbol{r},\omega)\boldsymbol{\varphi}_{njk} \\ &= \sum_{k=1}^{m}\sum_{j=1}^{N} i\omega \boldsymbol{Q_j}(\omega)\boldsymbol{ATV_k}(\boldsymbol{r},\omega)\boldsymbol{\varphi}_{njk} \\ &= \sum_{k=1}^{m} \boldsymbol{ATV_k}(\boldsymbol{r},\omega)v_{nk}(\omega) \\ &= \sum_{k=1}^{m} \boldsymbol{p_k}(r,\omega),\end{aligned} \tag{9}$$

where m is the total number of nodes; k is the node number; $\boldsymbol{ATV_k}(\boldsymbol{r},\omega)$ is the ATV of the kth node; $\varphi_{\boldsymbol{njk}}$ is the normal modal displacement of the kth node in the jth mode; $\boldsymbol{p_k}(r,\omega)$ is the sound pressure caused by the vibration of the kth node.

Assuming that panel structure c is composed of L nodes, the sound pressure $\boldsymbol{p_c}(\boldsymbol{r},\boldsymbol{\omega})$ caused by the vibration of the panel structure is given by Eq. (10).

$$\boldsymbol{p_c}(\boldsymbol{r},\omega) = \sum_{k=1}^{L} \boldsymbol{p_k}(\boldsymbol{r},\omega). \tag{10}$$

The panel acoustic contribution $D_c(\boldsymbol{r},\omega)$ of this structure is shown in Eq. (11).

$$D_c(\boldsymbol{r},\omega) = \frac{|\boldsymbol{p_c}(\boldsymbol{r},\omega)|\cos(\theta_p - \theta_c)}{|\boldsymbol{p}(\boldsymbol{r},\omega)|}, \tag{11}$$

where θ_c is the phase of $p_c(\boldsymbol{r},\omega)$.

The physical meaning of PAC is the proportion of the sound pressure generated by the vibration of the panel to the total sound pressure under a certain excitation. The greater the acoustic contribution of a panel, the greater the influence of the normal vibration of the panel on the total sound pressure.

2.4 Structural Topology Optimization Model

Generally, the location of the observation points, the density and wave velocity of the acoustic medium, and the calculation and analysis frequency will not change in the radiation noise calculation model. Therefore, even if the surface structure of a certain gearbox is slightly changed, the size and distribution of the ATV will not be affected. The main factor that has a significant influence on the radiation noise is the normal vibration velocity of the gearbox structure surface. In summary, in the region where the distribution of the ATV on the structure surface is large, the effective sound pressure of the corresponding field point can be reduced only by reducing the normal vibration speed of the region with the largest contribution. Essentially, it is better to apply the topology optimization method to solve this kind of target. Therefore, this study applies the topology optimization equation to reduce the normal vibration velocity in this region, and the corresponding topology optimization model [31] is shown in Eq. (12).

$$\begin{cases} \text{Optimization target}: \min\limits_{\rho_e} \|v_{ns}(\omega)\| \\ \text{Constraint conditions}: \\ \qquad V_s \le 30\%\text{V} \\ \qquad \|v_{nk}(\omega)\| < \eta\|v_{n0}(\omega)\| \\ \qquad (k = 1, 2, 3 \ldots s-1, s+1 \ldots N)(\eta < 1) \\ \text{Design space}: \ 0.01 \le \rho_e \le 1 \end{cases} \tag{12}$$

where $\boldsymbol{v}_{ns}(\omega)$ represents the normal vibration velocity of node s in the finite element model of a gearbox, which is located in the region with the largest acoustic contribution to the target field point, and the normal vibration velocity of this node in the original structure is greater than that of all other nodes in the region with the largest acoustic contribution. $\boldsymbol{v}_{n\mathrm{k}}(\omega)$ represents the normal vibration velocity at node k in the finite element model of gearbox, which is located in the region with the largest acoustic contribution to the target field point. η indicates the speed limiting coefficient, which is used to control the normal vibration speed of each node in the region with the largest acoustic contribution. $\boldsymbol{v}_{n0}(\omega)$ is the minimum normal vibration velocity in the region with the largest acoustic contribution to the target field point , which is constant during topology optimization. N represents the total number of nodes in the region with the largest acoustic contribution to the target field point. ρ_e is the volume density, which is a design variable in the topology optimization model.

3 Radiation Noise Prediction

3.1 Radiation Noise Prediction Process

The process diagram of gearbox-radiated noise analysis is shown in Figure 1. To simplify the study, the gear system was decoupled from the gearbox, and the dynamic load of the bearing was obtained by solving the dynamic equation. The gear system was used as the excitation source of the gearbox to solve its radiated noise. First, the complex solid model of the gearbox was simplified using 3D modeling software. The simplified solid model was imported into the finite element analysis software to obtain a finite element model for modal analysis, and the natural frequency and main mode shape of the gearbox system were obtained. Second, based on modal analysis, the vibration response of the gearbox was analyzed by applying the bearing dynamic load data, and the modal participation factor was obtained. Subsequently, based on the finite element model, the boundary element and sound field

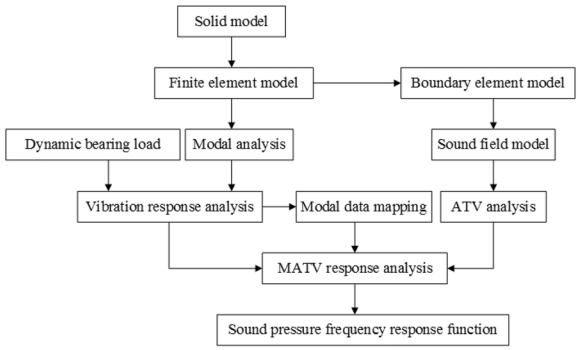

Figure 1 Radiated noise analysis process of gearbox

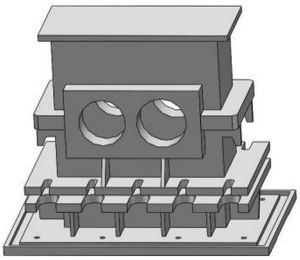

Figure 2 Solid model of gearbox

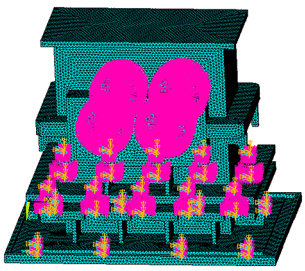

Figure 3 Finite element model of gearbox

Table 1 The first 20 natural frequencies of gearbox

Order	Frequency(Hz)	Order	Frequency(Hz)
1	89.669	11	1322.4
2	132.76	12	1368.8
3	151.00	13	1560.6
4	907.76	14	1721.3
5	917.01	15	1755.2
6	988.63	16	1759.7
7	1047.9	17	1788.4
8	1073.9	18	1829.3
9	1230.9	19	1840.6
10	1270.9	20	1856.0

mesh models were established for calculating the ATV. Finally, the sound response was calculated using the MATV method to obtain the sound pressure frequency response function of the field point.

3.2 Modal Analysis

This study adopts a simplified model of a gearbox, and its basic dimensions are length × width × height = 714 mm × 372 mm× 681 mm, as shown in Figure 2. Some small features in the structure were removed for proper simplification in the structural modeling. The gear transfer system is a single-stage herringbone gear transfer system that stimulates the box body through four sliding bearing seats. The box body was made of cast steel, with a Young's modulus of 210 GPa, Poisson's ratio of 0.3, and mass density of 7800 kg/m^3. The four-node tetrahedral element Solid285 was used to mesh the structure with a mesh size of 10 mm, and a total of 90482 nodes and 368771 elements were generated.

In the process of establishing the finite element model, the bearing hole center node and the upper and lower center nodes at the bolt hole of the machine foot were established. The nodes were assigned MASS21 mass elements with real constants MASSX, MASSY, and MASSZ, which were all 1×10^{-6}. A rigid coupling relationship was established between the bearing hole center node and inner wall surface node. Excitation could be applied to the box when a bearing dynamic load was applied. A COMBIN14 spring element with a longitudinal direction stiffness of 2×10^9 N/m was established between the upper and lower nodes of the pedestal bolt hole to simulate the pedestal bolt. This restricted the six degrees of freedom of the nodes of the spring element and simulated the installation state of the pedestal. The gearbox and base were connected by a vibration isolator, which was simplified as a spring unit with a spring stiffness of 6.67×10^6 N/m. The finite element model obtained after gearbox pretreatment is shown in Figure 3.

Modal analysis of the finite element model of the gearbox was performed using the Block Lanczos method. The working condition of the gearbox was 1600 r/min and the torque was 1066 N·m. Therefore, the peak frequency of the dynamic load of the bearing on the gearbox was 613.33 Hz, and its 6-times frequency was 3680 Hz. Considering that the 6-times frequency is less than the 100th natural frequency (4032 Hz), the natural frequency and mode shape of the first 100th order were calculated to meet the requirements of the subsequent mode-based forced response calculation. The first 20 orders of the natural frequencies of the gearbox are listed in Table 1.

3.3 Solving ATV

The acoustic boundary element model of the gearbox was based on a finite element model. The boundary element required a face mesh (2D mesh) rather than a solid mesh (3D mesh). Therefore, the surface elements of the finite element solid mesh were first extracted, and then shell elements were used to patch the bearing and bolt holes. Thus, the entire gearbox became a closed body, and it was convenient to calculate the radiated noise of the external sound field of the gearbox. Finally, the surface elements were extracted again and the mesh was coarsened to obtain a regular boundary element model. The working condition of the gearbox was 1600 r/min, and the torque was 1066 N·m. Considering that the peak frequency of the dynamic load of the bearing on the gearbox was 613.33 Hz, its 6-times frequency was 3680 Hz. Therefore, according to Eq. (13) [24], the BEM grid size was set to 15 mm, and its upper limit frequency was 3777.78 Hz. Figure 4 shows the BEM model as the basis for acoustic calculation.

$$L \leq \frac{c}{6f}, \tag{13}$$

where L is the boundary element grid size; c refers to the propagation speed of sound in the fluid medium, where the sound speed is 340 m/s; f is the highest frequency of the calculation.

Based on the boundary element model and considering the actual installation position of the gearbox, the reflecting surface and box sound field were determined. The sound speed was 340 m/s, and the air density was 1.225 kg/m^3. First, a reflecting plane was inserted to simulate the ground. Next, a box sound field mesh was defined. Finally, 1 m from the upper, front, left, and right sides of the sound field boundary was taken as the sound field measuring points for radiated noise, as shown in Figure 5. Furthermore, the ATV was introduced to improve the calculation efficiency, wherein different frequencies were calculated using the asynchronous distance. Finally, the ATV of the gearbox boundary-element model at different frequencies were obtained.

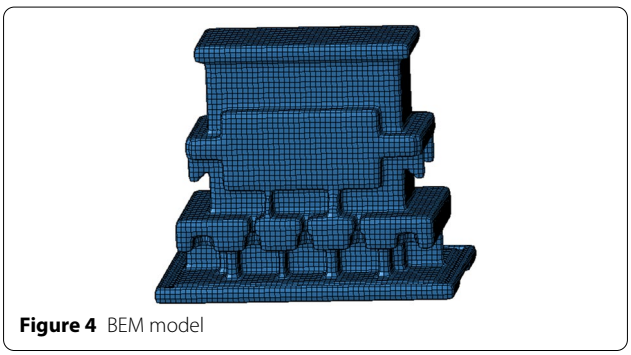

Figure 4 BEM model

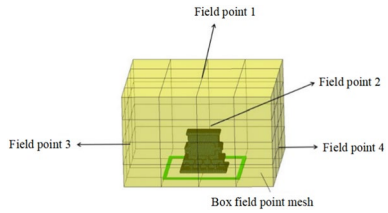

Figure 5 Sound field model

3.4 Gearbox Radiation Noise Prediction

Based on the modal analysis result, the dynamic load of the bearing was applied to the center node of the bearing hole, the modal superposition method was used to calculate the forced response, and the modal participation factor was obtained. Because the MATV method was used to calculate radiation noise, the modal participation factor was solved by the finite element model, whereas the ATV was solved using the boundary element model; therefore, it was necessary to transfer modal data from the finite element model to the boundary element model. The MATV acoustic response solution was calculated based on the ATV, modal data, and modal participation factor. Finally, the frequency response function at the field point was obtained.

The effective sound pressure level of the radiated noise at each field point is listed in Table 2 by solving the sound pressure frequency response function of the field point under the working. Table 3 lists the sound pressure levels of the radiated noise at the mesh frequency and mesh frequency doubling of each field point. According to the data presented in Table 2, the effective sound pressure level of field point 1 was the largest; therefore, this field point is selected as the optimization target field point. According to the data presented in Table 3, the radiated noise sound pressure level at the mesh frequency (613.33 Hz) was greater than that at other doubling frequencies; therefore, the mesh frequency (613.33 Hz) was selected as the optimized frequency.

Table 2 Effective sound pressure level of radiated noise at each field point (dB(A))

	Field point 1	Field point 2	Field point 3	Field point 4
Effective sound pressure level	95.19	92.61	85.79	84.23

Table 3 Radiation noise sound pressure level of each field point at meshing frequency and frequency doubling (dB(A))

Frequency	Field point 1	Field point 2	Field point 3	Field point 4
Meshing frequency	97.28	94.86	87.90	86.37
2-times mesh frequency	69.89	69.34	62.42	72.92
3-times mesh frequency	67.7	77.48	68.17	71.34

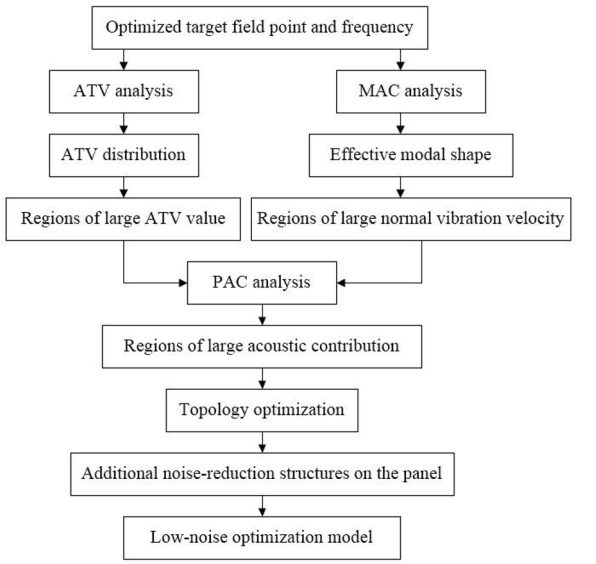

Figure 6 Low-noise optimization design process

4 Low-noise Optimization Design

4.1 Optimization Design Process

The low-noise optimization design process for the gearbox is shown in Figure 6. The first step was to determine the optimized target field point and frequency. The second step was to determine the region with a large ATV value through ATV analysis. In the third step, the mode with a large acoustic contribution was determined by MAC analysis, and the region with a large normal vibration speed was determined by analyzing the corresponding main vibration mode. In the fourth step, the panel was divided into the region where the ATV and normal vibration velocity were both large, and the panel with the largest acoustic contribution was determined by PAC analysis. The region with the largest PAC was that with the largest acoustic contribution. In the fifth step, a topology optimization model was established with the goal of reducing the normal vibration speed in this region. In the sixth step, according to the topology optimization results, noise reduction structures were added to the panel and a gearbox low-noise optimization model was established.

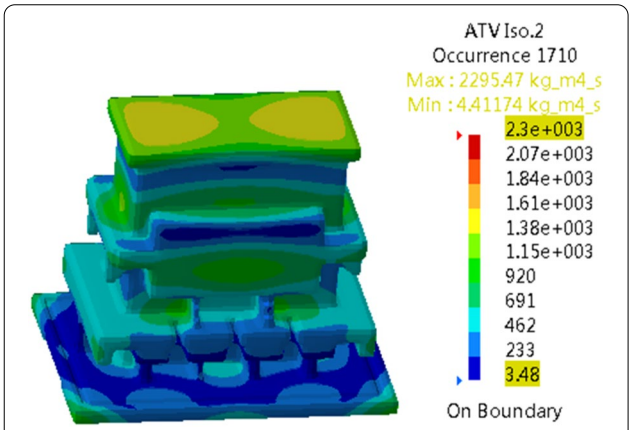

Figure 7 The distribution of ATV for field point 1 at 920 Hz

4.2 ATV Analysis

After the radiation noise calculation was completed, the ATV distribution corresponding to field point 1 at 920 Hz was obtained, as shown in Figure 7. It can be observed that the ATV on the top surface of the gearbox is far larger than that of the other surfaces. Therefore, the first screening result for the optimization region is shown in the top panel.

4.3 MAC Analysis

After the ATV analysis was completed, regions that may have a larger acoustic contribution could be identified by MAC analysis. Based on the analysis of the first 100 order modal results, the first 9th order mode with a larger absolute contribution to the sound pressure level at field point 1 was extracted, as shown in Figure 8. As can be seen from Figure 8, the contributions of the fifth and seventh modes to the modal acoustics of field point 1 were greater, reaching 40.01% and 4.66%, respectively, which indicates that the total sound pressure ratio of these two modes was the largest. The MAC of the other modes were all lower than 4% or even negative. Based on the results, the 5th and 7th modal shape diagrams were extracted, as shown in Figure 9. It can be observed from Figure 9 that the top surface and bearing pedestal regions theoretically have a relatively large normal vibration velocity.

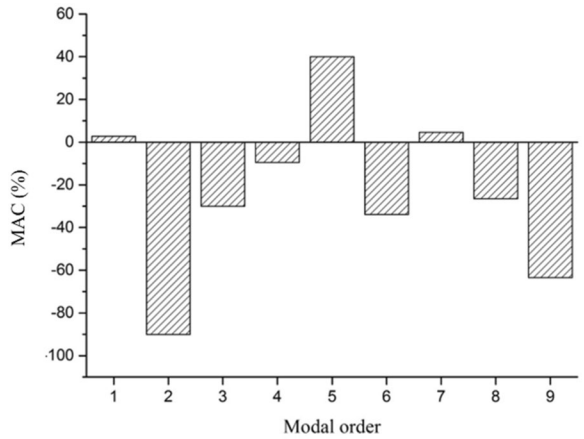

Figure 8 Results of MAC analysis of field point 1

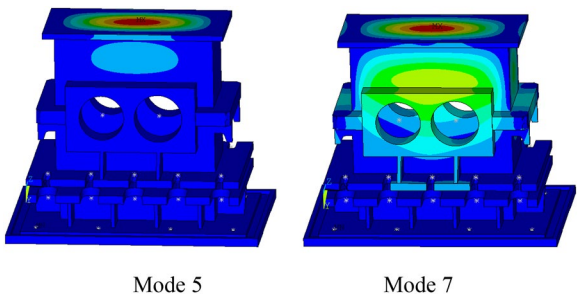

Figure 9 5th and 7th order modal shape diagrams

Combined with the ATV distribution nephogram in Figure 7 and the modal shape diagram in Figure 9, the acoustic contributions of the top surface of the gearbox and the bearing pedestal region at field point 1 were much greater than those of the other regions. Therefore, the second screening results of the optimization region were the top surface and bearing pedestal regions.

4.4 PAC Analysis

The panel with the maximum acoustic contribution could be determined by PAC analysis. Therefore, according to the analysis results of the ATV and MAC, the two panels were divided, as shown in Figure 10. The results of the PAC analysis are shown in Figure 11. It can be observed from Figure 11 that the acoustic contribution of panel 1 to field point 1 was much greater than that of panel 2. Therefore, the third screening result of the optimization region is shown in panel 1.

4.5 Structural Topology Optimization

According to the analysis of the ATV, MAC, and PAC, the region with the largest acoustic contribution to field point 1 is panel 1. Therefore, panel 1 was selected as the topology optimization region. The gearbox topology optimization model was established by reducing the normal vibration speed in the optimization region as the goal and constraint conditions, as shown in Figure 12. The topology optimization result cloud diagram

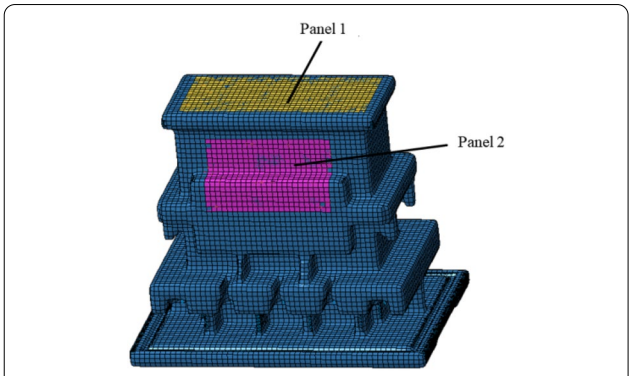

Figure 10 Panel division results

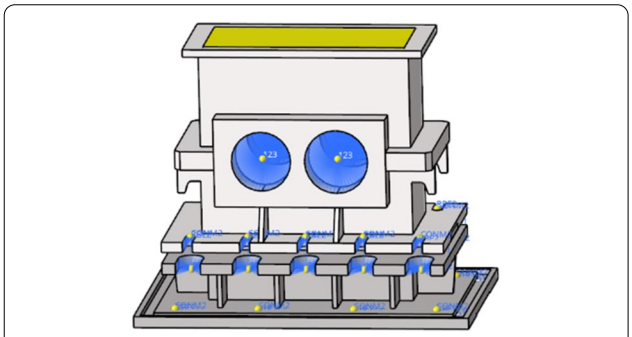

Figure 11 Results of PAC analysis

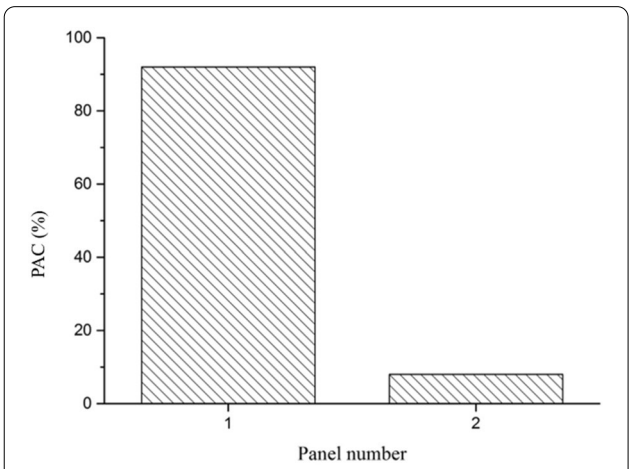

Figure 12 Noise reduction topology optimization model of single-stage gearbox for field point 1

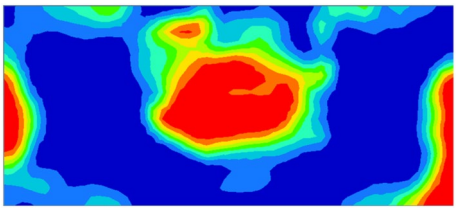

Figure 13 Results of noise reduction topology optimization of single-stage gearbox for field point 1

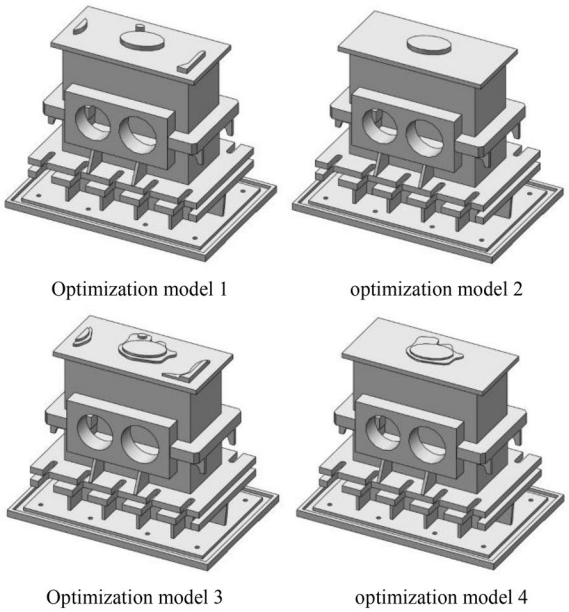

Figure 14 Optimal design model of noise reduction for single-stage gearbox

was obtained by solving the above model, as shown in Figure 13.

4.6 Structure Improvement Design for Noise Reduction

According to the topology optimization results, the gearbox was designed by adding noise reduction structures. The higher the bulk density of the materials, the more important the materials are. In the structural improvement design, the addition of materials should be prioritized in the optimization region. According to engineering experience, the thickness of the additional structures is 2.5 times that of panel 1. Therefore, four optimization models were designed, as shown in Figure 14. The additional structure thicknesses of optimization models 1 and 2 were 20 mm. Optimization model 1 considered all the red regions in the density nephogram, and optimization model 2 considered only the central red region of the density nephogram compared with optimization model 1. Compared with optimization model 1, optimization model 3 considered the red, yellow, and green regions in the density nephogram and set up stepped structures with a thickness of 7 mm; the additional structures of the two models have the same quality. Compared with optimization model 2, optimization model 4 considered the red, yellow, and green regions in the density nephogram and set stepped structures with a thickness of 7 mm; the additional structures of the two models having the same quality.

The radiation noise of the four optimization models was calculated, and the effective sound pressure level of the radiation noise at each field point was obtained, which was compared with the original model of the gearbox.

From the data presented in Table 4 shows that compared with the original model, the effective sound pressure levels of the radiated noise in the four fields of optimized models 1, 2, 3, and 4 are all reduced, which indicates the effectiveness of the low-noise optimization design of the gearbox.

Compared with the original model, optimized model 1 was reduced by 12.37 dB(A), 6.47 dB(A), 5.28 dB(A) and 2.27 dB(A), respectively, and the average value of effective sound pressure level of radiated noise at each site was reduced by 7.10 dB(A). Compared with the original gearbox model, optimized model 2 was reduced by 13.55 dB(A), 6.16 dB(A), 5.16 dB(A) and 4.11 dB(A), respectively, and the average value of effective sound pressure level of radiated noise at each field was reduced by 7.25

Table 4 Effective sound pressure level of radiated noise at each field point before and after topology optimization design of single-stage gearbox (dB(A))

	Field point 1	Field point 2	Field point 3	Field point 4	Average value
Original model	95.19	92.61	85.79	84.23	89.46
Optimization model 1	81.82	86.14	80.51	80.96	82.36
Optimization model 2	81.64	86.45	80.63	80.12	82.21
Optimization model 3	84.04	86.76	81.76	81.05	83.40
Optimization model 4	84.47	86.27	81.48	81.24	83.37

dB(A). Compared with optimization model 1, the difference of radiation noise results of optimization model 2 was less than 1 dB(A), which shows that the noise reduction effect can be achieved only by adding noise reduction structures in the center of the density nephogram. Therefore, optimization model 2 was selected for subsequent test verification.

Compared with the original model, optimized model 3 was reduced by 11.15 dB(A), 5.85 dB(A), 4.03 dB(A) and 3.18 dB(A), respectively, and the mean value of the effective sound pressure level of radiated noise at each site was reduced by 6.05 dB(A). Compared with the original gearbox model, optimized model 4 was reduced by 10.72 dB(A), 6.34 dB(A), 4.31 dB(A) and 2.99 dB(A), respectively, and the average effective sound pressure level of radiated noise at each field was reduced by 6.09 dB(A). Compared with optimization model 3, the difference in the radiation noise results of optimization model 4 was less than 1 dB(A), which shows that the noise reduction effect can be achieved only by adding noise reduction structures at the center of the density nephogram. Therefore, optimization model 4 was selected for subsequent test verification.

Based on the results of the topology optimization, there are approximately four locations where noise-reduction structures need to be added. However, according to the simulation results, the noise reduction effect can be achieved only by adding noise reduction structures at the center of the density nephogram. This is because the other three positions were located around plate surface 1, close to the fixing bolt, and its vibration was limited. Therefore, its acoustic contribution was also less than that of the central position.

5 Experimental Verification

5.1 Introduction of Test Bench

In this study, a mechanical power-flow closed test bench system was used to test the radiation noise of the test gearbox. The test bench was mainly composed of two test gearboxes, both of which were single-stage gearboxes driven by a herringbone gear. The two gearboxes were connected by high-speed torsion and rigid shafts, and low-speed torsion and rigid shafts, which were connected by rigid and diaphragm couplings, respectively. A loading coupling was added between the high-speed shaft and the accompanying test gearbox, and the driving motor was responsible for compensating the friction loss of the entire transfer system (see Figure 15).

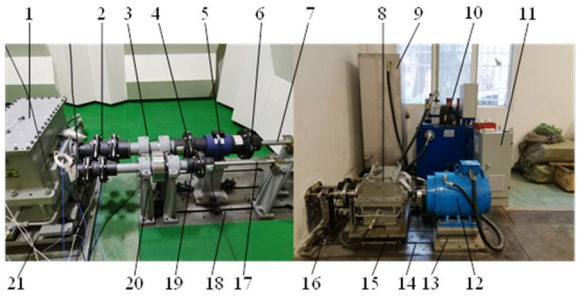

Figure 15 The mechanical power flow closed test bench. 1. Test gearbox, 2,4,6. Diaphragm coupling, 3. Low-speed shaft support seat, 5. Torque tachometer, 7. Low-speed torsion shaft, 8. Accompanying test gearbox, 9. Water pump, 10. Oil pump, 11. Frequency converter, 12. Motor, 13. Motor support seat, 14, 18. Basic platform, 15. Accompanying test gearbox base, 16. Load coupling, 17. High-speed torsion shaft, 19. Rigid coupling, 20. High speed shaft support seat, 21. Test gearbox base

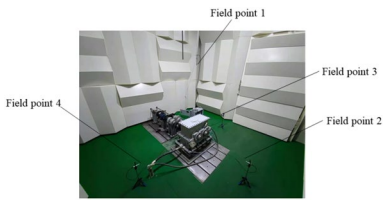

Figure 16 Sound field points layout of noise measuring

The test gearbox was placed in a semi-anechoic chamber. Four sound field test points were arranged around the test gearbox, and an acoustic sensor (type 130F20) was installed at the field point. The position of the sound field test point is consistent with that of the simulation model, as shown in Figure 16.

By loading the coupling, a torque of 1066 N·m was applied, starting the motor, adjusting the motor to low speed, and gradually adjusting the motor speed to 2000 r/min after the test gearbox ran smoothly. Then, the sound pressure signals were collected using the MI-8014 data acquisition system of the ECON Technologies Company. Finally, the data were processed using an offline analysis software.

Table 5 Comparison of simulated and measured values of effective sound pressure level of radiated noise at four field points in test gearbox (dB(A))

Field point	Field point 1	Field point 2	Field point 3	Field point 4	Average value
Simulated values	95.19	92.61	85.79	84.23	89.46
Measured values	93,15	89.96	83.94	82.96	87.50
Distance	2.04	2.65	1.85	1.27	1.96

5.2 Experimental Verification of Radiation Noise Prediction Method

The measured and simulated values of the effective sound pressure level of the test gearbox at four field points are listed in Table 5, where the speed is 1600 r/min and the torque is 1066 N·m. It can be seen from the data presented in Table 5 that the differences between simulated and measured values of field point 1, 2, 3, and 4 are 2.04 dB(A), 2.65 dB(A), 1.5 dB(A), and 1.27 dB(A), respectively, which do not exceed 3 dB(A). The validity of the radiated noise prediction model and method was demonstrated.

5.3 Experimental Analysis of Low-noise Optimization Design Method

When the speed was 1600 r/min and the torque was 1066 N·m, the measured values of the effective sound pressure level of the radiated noise at four field points before and after the optimization of the test gearbox are shown in Table 6. It can be seen from the data presented in Table 6 that after the low-noise optimization design of the test gearbox, the measured values of optimization model 2 and 4 decreased by 9.41 dB(A) and 7.28 dB(A), respectively, compared with the original model at field point 1, and the average measured value of each field point decreased by 2.64 dB(A) and 2.54 dB(A), respectively.

The radiated noise of the gearbox before and after optimization was measured in a semi-anechoic chamber using a mechanical power flow closed test bench. The effectiveness of the low-noise optimization design method was verified by comparing the simulation results with the measurement results.

The measured values of the A-weighted 1/3 octave sound pressure level of the radiated noise at each field point are shown in Figure 17. It can be seen that the radiated noise of field point 1 decreased in the 630 Hz band, which includes the meshing frequency (613.33 Hz). The measured values of radiated noise in other frequency bands changed slightly because the target frequency of low-noise optimization is the meshing frequency (613.33 Hz). The measured value of the radiated noise of field points 2, 3, and 4 changed slightly because the low-noise optimization target field point was field point 1. This shows that the low-noise structure optimization design method proposed in this study is effective.

6 Conclusions

(1) Considering the dynamic excitation of a gear system, the A-weighted radiated noise sound pressure level of each field point of the gearbox was calculated based on the MATV method. The validity of the radiated noise prediction method was verified by comparing the simulation and measurement values.

(2) According to the results of the topology optimization, four types of noise reduction structures were added to the gearbox, and four types of gearbox low-noise optimization models were established. Based on the noise simulation results and experimental verification, the validity of the low-noise optimization design method of the gearbox was verified. The noise-reduction effect can be achieved only by adding noise-reduction structures at the center of the density nephogram.

Table 6 Comparison of measured values of effective sound pressure level of radiated noise at four field points before and after optimization of test gearbox (dB(A))

	Field point 1	Field point 2	Field point 3	Field point 4	Average value
Original model	93.15	89.96	83.94	82.96	87.50
Optimization model 2	83.74	88.35	82.73	84.62	84.86
Optimization model 4	85.87	88.15	82.78	83.07	84.97

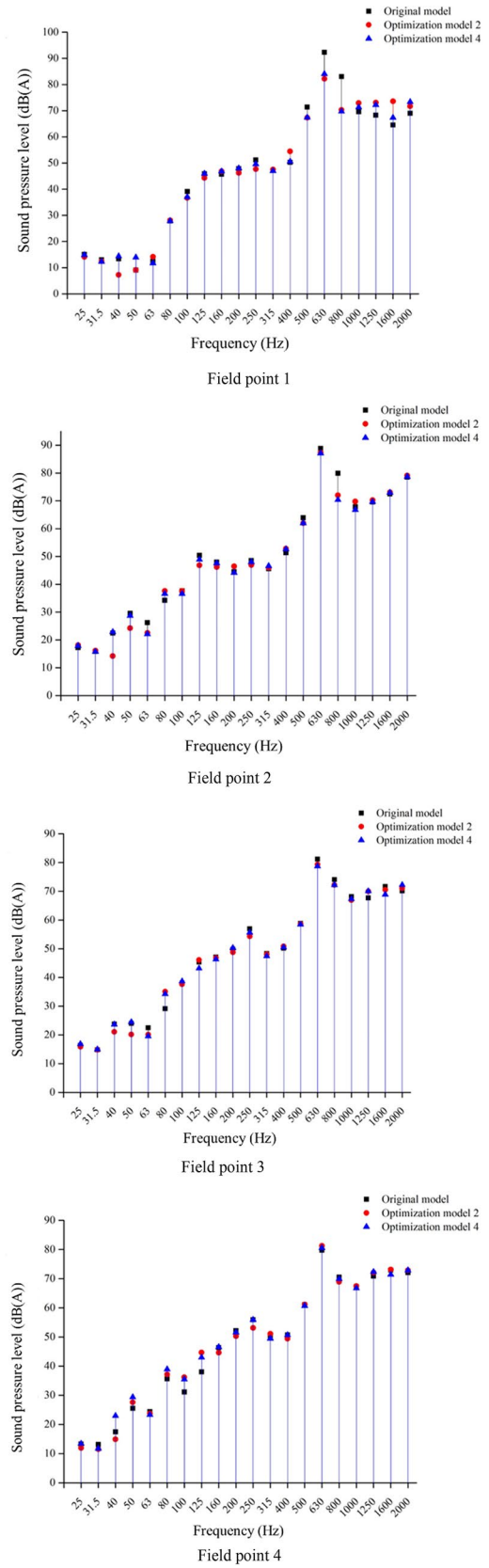

Figure 17 The measured value of A-weighted 1/3 octave sound pressure level of radiated noise at each field point

Acknowledgements
Not applicable.

Author contributions
LL, KK and ZH proposed the radiated noise prediction method and gearbox low-noise optimization method. LL, KK wrote the manuscript. KK, YX and JG were in charge of the entire experiment. LL and GL checked and improved the manuscript in writing. All authors read and approved the final manuscript.

Authors information
Lan Liu, born in 1974, is currently an associate professor and master tutor at *Shaanxi Engineering Laboratory for Transmissions and Controls, School of Mechanical Engineering, Northwestern Polytechnical University, China*. His main research interests include mechanical system dynamics, finite element analysis, noise prediction technology and analysis method of gear transmission mechanism.
E-mail: liulan@nwpu.edu.cn
Kun Kang, born in 1996, is currently a master candidate at *Shaanxi Engineering Laboratory for Transmissions and Controls, School of Mechanical Engineering, Northwestern Polytechnical University, China*.
E-mail: 2019201154@mail.nwpu.edu.cn
Yingjie Xi, born in 1997, is currently a master candidate at *Shaanxi Engineering Laboratory for Transmissions and Controls, School of Mechanical Engineering, Northwestern Polytechnical University, China*.
E-mail: 2020261550@mail.nwpu.edu.cn
Zhengxi Hu, born in 1996, is employed in *Xi'an Aerospace Dynamic Test Technology Research Institute, Xi'an, China*. He received his master's degree from *Northwestern Polytechnical University, China*, in 2021.
E-mail: hu15635997252@163.com
Jingyi Gong, born in 1992, is currently a PhD candidate at *Shaanxi Engineering Laboratory for Transmissions and Controls, School of Mechanical Engineering, Northwestern Polytechnical University, China*. He received his master degree from *Southwest University, China*, in 2018. His research interest is gear system dynamics.
E-mail: 2018100485@mail.nwpu.edu.cn
Geng Liu, born in 1962, is currently a professor and PhD candidate supervisor at *Shaanxi Engineering Laboratory for Transmissions and Controls, School of Mechanical Engineering, Northwestern Polytechnical University*, China. His main research interests include mechanical system dynamics, electromechanical actuation system, contact mechanics.
E-mail: npuliug@nwpu.edu.cn

Funding
Supported by National Key R&D Program of China (Grant No. 2018YFB2001501) and Key Program of National Natural Science Foundation of China (Grant No. 51535009).

Competing interests
The authors declare that they have no competing interests.

Author Details
[1]Shaanxi Engineering Laboratory for Transmissions and Controls, School of Mechanical Engineering, Northwestern Polytechnical University, Xi'an 710072, China. [2]Xi'an Aerospace Dynamic Test Technology Research Institute, Xi'an 710072, China.

Received: 5 August 2021 Revised: 19 June 2022 Accepted: 14 September 2022
Published online: 25 October 2022

References

[1] L Lin, M S Yu, T X Fu. A review of control and design techniques for acoustic stealth of surface ships. *Ship Science and Technology*, 2005, 27(2): 92-96. (in Chinese)
[2] J Tuma. Gearbox noise and vibration prediction and control. *International Journal of Acoustics and Vibration*, 2009, 14(2): 99-108.
[3] A R Mohanty, B D S Pierre, P Suruli-Narayanasami. Structure-borne noise reduction in a truck cab interior using numerical techniques. *Applied Acoustics*, 2000, 59(1): 1-17.
[4] Y N Liu, L Liu, G Liu, et al. Layout method of damping material for gearbox based on acoustic contribution. *Journal of Northwestern Polytechnical University*, 2019, 37(4): 757-766. (in Chinese)
[5] Y C Liu. *Research on interior sound quality based on the contribution of body panel*. Zhenjiang: Jiangsu University, 2020. (in Chinese)
[6] J P Wang, S Chang, G Liu, et al. Gearbox noise reduction based on modal acoustic contributions. *Journal of Vibration and Shock*, 2015, 34(17): 50-57. (in Chinese)
[7] J P Wang, M Song, X Wang, et al. A structural design method of gearboxes with low noise at multi-field points by combining acoustic contribution and topology optimization. *Journal of Vibration and Shock*, 2021, 40(16): 61-68. (in Chinese)
[8] B F Zong, C M Chu, C Huang, et al. Study on acoustic contribution analysis method of automobile transmission housing. *Journal of Mechanical Strength*, 2019, 41(2): 493-498. (in Chinese)
[9] J B Du, N Olhoff. Topological design of vibrating structures with respect to optimum sound pressure characteristics in a surrounding acoustic medium. *Structural and Multidisciplinary Optimization*, 2010, 42(1): 43-54.
[10] Y W Wang, R W Lei, H Wang. Structural topology optimization of flying wing aircraft. *Journal of Beijing University of Aeronautics and Astronautics*, 2022, 25(4): 1-13. (in Chinese)
[11] L Tan, B Cheng, D Jia, et al. Topology optimization design of an aeroengine bracket under multiple load cases. *Aeroengine*, 2022, 48(2): 90-95. (in Chinese)
[12] L Wang, Z S Li, K X Gu, et al. Research on topology optimization method of rocket sled track structure under displacement constraint. *Aeronautical Science & Technology*, 2022, 33(2): 97-102. (in Chinese)
[13] H F Zhai, J J Hou, Z P Fang, et al. Research on lightweight design of the hub motor's shell structure based on topology optimization. *Journal of Machine Design*, 2022, 39(1): 105-110. (in Chinese)
[14] Z F Zhang, Q B Yin, Z Chen, et al. Topology optimization of car body damping materials based on transfer path analysis. *Noise and Vibration Control*, 2022, 42(2): 167-172. (in Chinese)
[15] J L Liu, N H Zhu. The lightweight design of H-beam web section based on topology optimization. *Chinese Journal of Applied Mechanics*, 2021, 38(6): 2275-2283. (in Chinese)
[16] J Q Zhan, Y T Wang, M Liu, et al. Topological design of compliant mechanisms with hybrid constraints. *Journal of Vibration and Shock*, 2022, 41(4): 159-166. (in Chinese)
[17] W Wang, Q L Zhang, Y S Xu. Topology optimization method based on dynamic Gaussian sensitivity filtering. *Computer Integrated Manufacturing Systems*, 2022, 29(4): 1-22. (in Chinese)
[18] J J Fu, Y Zhang, Y X Du, et al. Eigenvalue topology optimization of periodic cellular structures. *Journal of Vibration and Shock*, 2022, 41(3): 73-81. (in Chinese)
[19] J K Zhou, L J Xia, K Y Huang. Design-oriented topology optimization of structures. *Journal of Ship Mechanics*, 2022, 26(4): 538-546. (in Chinese)
[20] X P Zhu, L Chen, J Huang. A novel unit cell boundary condition of mathematical homogenization method for periodical composite structure. *Chinese Journal of Computational Mechanics*, 2021, 38(3): 401-410. (in Chinese)
[21] Z X Yang, X P Ying, J Yan, et al. Study of equivalent mechanical properties of corrugated structure based on asymptotic homogenization method. *Journal of Dalian University of Technology*, 2021, 61(5): 498-505. (in Chinese)
[22] N Pollini, O Amir. Mixed projection- and density-based topology optimization with applications to structural assemblies. *Struct. Multidisc Optim.*, 2020(61): 687–710.
[23] W J Shang, W Xue, Y D Xu, et al. Undersea buried pipeline reconstruction based on the level set and inverse multiquadric regularization method. *Journal of Ocean University of China*, 2022, 21(1): 101-112.
[24] Y T Jiang, M Zhao. Topology optimization of underwater pressure structure design with parametric level set method. *Journal of Ship Mechanics*, 2022, 26(3): 400-413. (in Chinese)
[25] J Park, S Y Wang. Noise reduction for compressors by modes control using topology optimization of eigenvalue. *Journal of Sound and Vibration*, 2008, 315: 836-848.
[26] L Shu, Z D Fang, G J Zhao. Topology optimization design for vibration and noise reduction of cab structure. *Vibration and Shock*, 2008, 27(3): 113-116. (in Chinese)
[27] H K Li, C Guo, S L Fang, et al. Research on optimal design method of vibration and noise reduction of gearbox. *Vibration and Shock*, 2013, 32(17): 150-154. (in Chinese)
[28] Y Zhang, Y Q Cao. Noise control in car based on multi-objective dynamics topology optimization of damping layer. *Journal of Chongqing Jiaotong University*(*Natural Science*), 2019, 38(10): 121-126. (in Chinese)
[29] Z G Li, F L Zhan. *Virtual. Lab Acoustics. Advanced application examples of acoustic simulation calculation*. Beijing: National Defense Industry Press, 2010. (in Chinese)
[30] Z H Ni. *Mechanics of vibration*. Xi 'an: Xi 'an Jiaotong University Press, 1988. (in Chinese)
[31] J P Wang, S Chang, G Liu, et al. Optimal rib layout design for noise reduction based on topology optimization and acoustic contribution. *Structural and Multidisciplinary Optimization*, 2017, 56(5): 1093-1108.